ELSEVIER

Journal of Fluids and Structures 21 (2005) 413–427

JOURNAL OF FLUIDS AND STRUCTURES

www.elsevier.com/locate/jfs

Hydrodynamic loads during initial stage of floating body impact

A.A. Korobkin[a], A. Iafrati[b,*]

[a]*Lavrentyev Institute of Hydrodynamics, Novosibirsk, Russia*
[b]*INSEAN-Istituto Nazionale per Studi ed Esperienze di Architettura Navale, Roma, Italy*

Received 29 November 2004; accepted 3 August 2005
Available online 6 October 2005

Abstract

Hydrodynamic loads acting on a floating flared body, which starts suddenly to move, are investigated by using both asymptotic and numerical methods. The initial stage of the body motion is of main concern in this paper. Analysis is performed within the approximation of two-dimensional potential flow of an ideal and incompressible liquid with negligible surface tension effects. Initially the body is in contact with liquid, the liquid free surface is horizontal and the body displacement during the initial stage is assumed prescribed as a function of time. The body is symmetric with respect to the vertical axis and can move only in the vertical direction. Initial asymptotics of the hydrodynamic loads acting on the moving body are derived. Nondimensional body displacement plays the role of the small parameter of the problem. It is shown that the force asymptotics are strongly dependent on the flow details close to the intersection points between the body surface and the liquid free boundary. In particular, the standard small time expansion procedure, which provides correct initial asymptotics of loads in the case of a fully submerged body, is not applicable to the problem of a partly submerged (floating) body. This is because, for floating bodies, noninteger powers of body displacement appear in the initial asymptotics of the loads. For bodies with deadrise angles at the water level smaller than 45°, negative powers have been discovered in the initial asymptotics. Fully nonlinear unsteady numerical simulations are carried out for a floating wedge, which starts suddenly to penetrate the water. A careful verification of the numerical results is performed aimed at identifying the initial part of the time history of the hydrodynamic loads which, due to the simplifying assumptions of the numerical approach, is not reliable. Asymptotic analysis is used for interpretation of the numerical results. A fairly good agreement between the theoretical and numerical predictions of the hydrodynamic loads just after the impact has been found. A practical method to derive the initial hydrodynamic loads, by using the results of direct numerical simulations of the floating body impact, is suggested.

Keywords: Free surface flows; Water impact; Asymptotic methods; Potential flows; Boundary element methods

1. Introduction

The initial stage of two-dimensional liquid flow caused by a sudden vertical motion of a body initially floating on a still liquid surface is considered. The body is assumed symmetric with respect to its vertical axis and flared. The angle

*Corresponding author. Tel.: +39 06 50299 296; fax: +39 06 507 0619.
E-mail address: a.iafrati@insean.it (A. Iafrati).

0889-9746/$ - see front matter © 2005 Elsevier Ltd. All rights reserved.
doi:10.1016/j.jfluidstructs.2005.08.002

between the tangent to the body contour at the water line and the initially horizontal free surface is denoted by γ, where $\gamma<\pi/2$ (see Fig. 1). The hydrodynamic loads during the early stage are of primary interest in the present analysis.

Hydrodynamic loads generated after sudden motions of bodies in water have received considerable attention. By using a small time expansion procedure, Tyvand and Miloh (1995) obtained the initial asymptotics of the loads acting on a circular cylinder. Fully nonlinear calculations of the free-surface deformations of the initially calm water caused by forced constant velocity motion of a totally submerged circular cylinder were performed in Moyo (1996) and compared with the small-time asymptotics obtained in Tyvand and Miloh (1995). The asymptotic results which are taken to third order, when the gravity terms first appear in the expansion, were found to be in excellent agreement with the numerical calculations for small times. Faltinsen (1977) and Vinje and Brevig (1980) evaluated numerically the hydrodynamic loads generated by the sudden vertical motion of a floating body. However, due to different ways adopted to describe the very early stage, significantly different results were obtained (see discussion in Vinje, 1994). With the aim of getting deeper insights into the flow generated by a floating body, Korobkin and Wu (2002) derived the initial solution generated by a sudden motion of a circular cylinder initially half-submerged into the liquid at rest. The sudden vertical motion of a flared body is even more complicated by the fact that in this case the first-order solution is already singular about the intersection point. The floating wedge impact problem has been investigated in Iafrati and Korobkin (2004) where the inner solution was derived through a suitable set of stretched variables.

In the present paper, the small time asymptotics of hydrodynamic loads acting on a floating flared body during the early stage after its sudden start is derived. The analysis is carried out by assuming the fluid to be ideal and incompressible, with negligible surface tension effects. Although compressibility of the liquid is disregarded in the present study, it is worth remarking that for floating bodies it matters only during a very short stage just after the impact instant (Korobkin and Pukhnachov, 1988). Duration of the compressibility stage is of the order of $\mathcal{O}(L/c_0)$ where L is the length scale of the body and c_0 is the sound speed in the resting liquid. It is convenient to take L/V_0 as the time scale of the process, where V_0 is the initial velocity of the body. In terms of the nondimensional time the duration of the compressible stage is of the order of $\mathcal{O}(M)$, where M is the Mach number, $M=V_0/c_0$. In many practical situations the impact velocity V_0 is much smaller than c_0, which indicates that the compressibility stage is of very short duration. In this study we are concerned with the initial stage, when $M\ll t\ll 1$; this is with the incompressible stage, which lasts much longer than the compressible one but still short enough so that the body displacement during this stage is very small compared with the characteristic body dimension L. If compressibility effects are not taken into account, one is forced to deal with flow velocities which change instantly at $t=0$ from zero to finite values, that is to deal with infinite accelerations and, correspondingly, with infinite hydrodynamic loads.

During the initial stage under consideration, the liquid flow is assumed potential. The velocity potential is obtained by using the method of matched asymptotic expansions. It is well known that the leading term of the flow velocity just after the impact is given by the pressure-impulse approach and has a singularity at the intersection points between the liquid free surface and the body contour. This is why an inner solution near the intersection points has to be derived and matched with the outer one. It should be noticed that the inner solution will give a contribution to the higher-order terms of the outer solution, modifying both the flow and the pressure distribution in the main flow region. The latter effect, which is a feedback of the flow near the water level to the flow in the main region, is of strong importance in the problem of flared body impact. It is shown that terms with non-integer power of body displacement, which are related to the eigensolutions of the inner problem, have to be included in the small time expansion of the outer pressure distribution. These non-integer powers are dependent on the deadrise angle γ at the water line and, for angles smaller than 45°, negative powers appear which are responsible for high hydrodynamic loads just after impact. Note that the pressure details in the inner region also provide their own contribution to the total hydrodynamic load on the moving body. The order of this contribution is estimated in this paper.

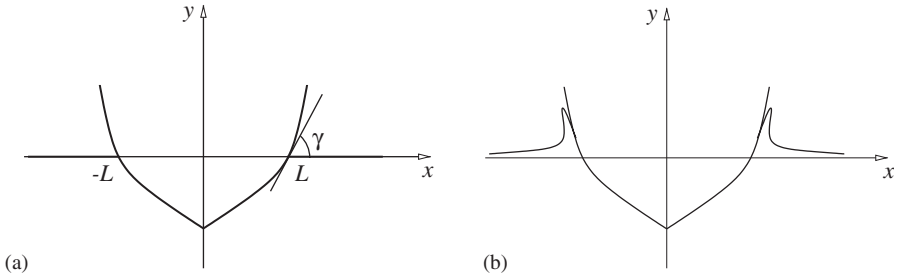

Fig. 1. Sketches of the body and free surface configurations at $t=0$ (a) and $t>0$ (b).

It should be noted that the present analysis is not valid for floating bodies with small deadrise angles, when the wetted area increases at a very high rate during the sudden vertical displacement of the body. The case of a floating wedge impact with small deadrise angle was studied in Oliver (2002) within the Wagner approach. The problem of very thin floating body impact corresponds, in the leading order, to the impact of a vertical plate. The initial asymptotic solution for the latter problem was given in King and Needham (1994). Neither the cases of small or large deadrise angles are considered in this paper.

In order to confirm the theoretical findings, a fully nonlinear unsteady numerical solver (Iafrati et al., 2000) is adopted to simulate the water entry of a two-dimensional wedge, partly submerged at $t = 0$, and to evaluate the resulting hydrodynamic loads. The model is based on a mixed Eulerian–Lagrangian formulation. The normal derivative of the velocity potential is assigned along the rigid body surface whereas the velocity potential on the free surface is obtained by integration in time of the unsteady Bernoulli equation. Hence, at each time step, the velocity potential is given in terms of a boundary integral representation and a boundary element approach is used to derive the velocity potential along the body contour and its normal derivative along the free surface.

As soon as the body starts to penetrate into the liquid, a jet develops about the intersection between the free surface and the body contour. Depending on the deadrise angle, the jet can become very thin, thus making its description very challenging. Although sophisticated methods have been recently developed to describe the flow inside the thin liquid layer (Battistin and Iafrati, 2004), even simple models (Zhao and Faltinsen, 1993; Battistin and Iafrati, 2003) provide accurate prediction of the total hydrodynamic load, since the pressure along the body portion in contact with the thin jet layer is very close to zero.

Independently of the model adopted to describe the flow in the thin jet layer, due to initial mismatch of the boundary conditions at the intersection point, an initial time interval exists during which hydrodynamic loads provided by numerical simulations are meaningless (Iafrati et al., 2000; Battistin and Iafrati, 2003). In the present work, numerical simulations with highly refined panel size are done in order to clearly identify the time stage where the predicted hydrodynamic loads are reliable. Then, the time history of the hydrodynamic load is interpolated by using the leading terms of the asymptotic behaviour theoretically derived. The rather good agreement found between the interpolated curve and the original numerical data proves the validity of the theoretical findings. For deadrise angles larger than 45°, the constant term of the time series theoretically derived agrees satisfactorily with the value provided by the interpolation of the numerical results.

The methodology adopted in this analysis is discussed in more detail in Section 8 with the aim of deriving a practical tool to correct numerical predictions of the hydrodynamic loads at the early stage of floating body motion.

2. Formulation of the problem

The unsteady two-dimensional flow generated by impulsive vertical motion of a body initially floating on a liquid free surface is considered. The liquid is at rest and its free surface is horizontal before the body starts to move. The body is assumed symmetric with respect to its vertical axis and flared. The angle between the tangent to the body surface at the water line and the initially horizontal liquid surface is denoted by γ, $\gamma < \frac{\pi}{2}$ (see Fig. 1(a)). The body width at the water level is $2L$.

At some instant of time, which is taken as the initial one, the body suddenly starts to penetrate the liquid with an initial velocity V_0. We take L and V_0 as length scale and velocity scale, respectively. Nondimensional variables are used below, with the ratio L/V_0 being the time scale of the process. The vertical displacement of the body is $h(t)$, where $h(0) = 0$ and $\dot{h}(0) = 1$, and an overdot stands for the time derivative. In the present analysis the function $h(t)$ is assumed given.

On the basis of the aforementioned assumptions, the irrotational flow caused by the impact is described by the complex velocity potential $w(z,t) = \varphi(x,y,t) + \mathrm{i}\psi(x,y,t)$, where $z = x + \mathrm{i}y$, $\varphi(x,y,t)$ is the velocity potential and $\psi(x,y,t)$ is the stream function. The complex potential $w(z,t)$ is an analytical function in the flow region $\Omega(t)$, decays at infinity, $x^2 + y^2 \to \infty$, and satisfies the following boundary conditions

$$\psi = \dot{h}(t)x \quad (y = f(x) - h(t)), \tag{1}$$

$$\varphi_t + \tfrac{1}{2}|\nabla\varphi|^2 + \mathrm{Fr}^{-2}\eta = 0, \quad \varphi_y = \eta_x\varphi_x + \eta_t \ \ (y = \eta(x,t)), \tag{2}$$

where equation $y = f(x)$ describes the shape of the floating body, $f(-x) = f(x), f(1) = 0, f'(1) = \tan\gamma$, the function $f(x)$ is smooth where $x > 0$. The Froude number in (2) is given as $\mathrm{Fr} = V_0/\sqrt{gL}$, where g is the gravitational acceleration.

Equation $y=\eta(x,t)$ describes the elevation of the liquid free surface (the function $\eta(x,t)$ can be multi-valued) and $\eta(-x,t)=\eta(x,t)$, $\eta(x,0)=0$ where $|x|>1$ and $\eta(x,t)\to 0$ as $|x|\to\infty$.

Once the velocity potential $\varphi(x,y,t)$ has been obtained, the hydrodynamic pressure $p(x,y,t)$ is calculated as

$$p(x,y,t)=-\varphi_t-\tfrac{1}{2}|\nabla\varphi|^2-\mathrm{Fr}^{-2}y, \tag{3}$$

with the pressure scale being $\varrho_0 V_0^2$, where ϱ_0 is the liquid density. The vertical force $F(t)$ acting on the moving body is given as

$$F(t)=\int_{WS(t)} p[x,f(x)-h(t),t]\,\mathrm{d}x, \tag{4}$$

where $WS(t)$ is the wetted part of the body surface. The force scale is $\varrho_0 V_0^2 L$. We shall determine the asymptotic behaviour of both the complex potential $w(z,t)$, $z=x+\mathrm{i}y$, and the hydrodynamic force $F(t)$ as $t\to 0$ up to the terms of the orders $o(t)$ and $o(1)$, respectively. Here $o(1)$ designates the terms which tend to zero and $o(t)$ the terms which tend to zero faster than t as $t\to 0$.

3. Small time solution

The solution of the problem is sought in the form

$$w(z,t)=\dot{h}(t)w_0(z)+w_1(z,t)+o(t), \tag{5}$$

where the first term corresponds to the pressure-impulse solution and the second term describes the evolution of the flow after the impact, $w_1(z,t)\to 0$ as $t\to 0$. According to the pressure-impulse theory, the potential $w_0(z)$ is an analytical and bounded function in $\Omega(0)$, decays at infinity and satisfies the boundary conditions

$$\Im[w_0]=x \quad (y=f(x),|x|<1), \qquad \Re[w_0]=0 \quad (y=0,|x|>1). \tag{6}$$

The complex potential $w_0(z)$ can be readily obtained once the conformal mapping $z=G(\zeta)$, $\zeta=\xi+\mathrm{i}\omega$, of the lower half-plane $\omega<0$ onto the domain $\Omega(0)$ is known. The conformal mapping is specified by the conditions $G(\pm 1-\mathrm{i}0)=\pm 1$ (see Fig. 2). The interval $|\xi|<1$, $\omega=0$ corresponds to the submerged part of the body contour and the rest of the real axis to the liquid free surface. Far from the body surface, $|\zeta|\to\infty$, the mapping behaves as $G(\zeta)=G_\infty\zeta+G_0/\zeta+\mathcal{O}(\zeta^{-3})$, where G_∞ and G_0 are real constants.

The analytic function $W_0(\zeta)=w_0[G(\zeta)]$ satisfies the boundary conditions

$$\Im[W_0]=x(\xi,0) \quad (\omega=0,|\xi|<1), \qquad \Re[W_0]=0 \quad (\omega=0,|\xi|>1), \tag{7}$$

where $x(\xi,\omega)=\Re[G(\zeta)]$, and is given as

$$W_0(\zeta)=\mathrm{i}\left[G(\zeta)-G_\infty\sqrt{\zeta^2-1}\right]. \tag{8}$$

The velocity potential $\varphi_0(x,y)=\Re[w_0(z)]$ on the body surface, $y=f(x)$, is given in parametric form

$$\varphi_0(x,f(x))=-f(x)-G_\infty\sqrt{1-\xi^2}, \quad x=x(\xi,0)\ (|\xi|<1). \tag{9}$$

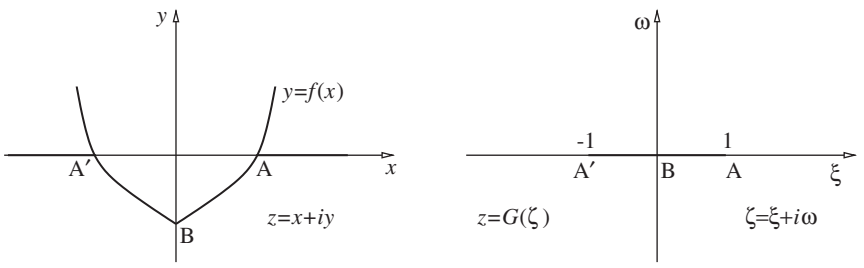

Fig. 2. Sketch of the body contour in the physical (z) and transformed (ζ) planes.

In the problem of floating plate impact, where $f(x) \equiv 0$, $|x|<1$, we obtain $G(\zeta) = \zeta$ and Eq. (9) takes the form

$$\varphi_0(x,0) = -\sqrt{1-x^2} \quad (|x|<1),$$

which is a well-known formula in the Wagner theory of impact.

The boundary-value problem for the second term in (5) can be obtained by substituting the small time expansion (5) into the body boundary condition (1) and the dynamic boundary condition (2) and omitting the terms of the orders $o(t)$ and $o(1)$, respectively. It should be noticed that the kinematic boundary condition (2) and decomposition (5) yield

$$\eta(x,t) = h(t)\eta_0(x) + \eta_1(x,t) + o(t^2). \tag{10}$$

The boundary conditions for the analytic function $w_1(z,t) = \varphi_1(x,y,t) + \mathrm{i}\psi_1(x,y,t)$ are imposed on the initial position of the body surface and that of the liquid free surface. We obtain

$$\psi_1 = h\dot{h}\varphi_{0x} + o(t) \quad (y = f(x), |x|<1), \tag{11}$$

$$\varphi_{1t} = -\tfrac{1}{2}\dot{h}^2(\varphi_{0y})^2 + o(1) \quad (y=0, |x|>1). \tag{12}$$

Special forms of the boundary conditions (11) and (12), decomposition (5) and asymptotic formula $h(t)\ddot{h}(t) = o(1)$ show that

$$w_1(z,t) = h\dot{h}\tilde{w}_1(z,t), \tag{13}$$

where the analytic function $\tilde{w}_1(z,t)$ is defined in $\Omega(0)$, decays at infinity and satisfies the boundary conditions

$$\tilde{\psi}_1 = \varphi_{0x} \quad (y=f(x), |x|<1), \qquad \tilde{\varphi}_1 = -\tfrac{1}{2}(\varphi_{0y})^2 \quad (y=0, |x|>1). \tag{14}$$

Note that the analytic function $[w_0'(z)]^2$ is equal to $-(\varphi_{0y})^2(x,0)$ on the free surface, $|x|>1$. This observation allows us to decompose the unknown function $\tilde{w}_1(z,t)$ as

$$\tilde{w}_1(z,t) = \tfrac{1}{2}\left[w_0'(z)\right]^2 + \hat{w}_1(z,t), \tag{15}$$

where the new analytic function $\hat{w}_1(z,t)$ satisfies the boundary conditions

$$\Im[\hat{w}_1] = \varphi_{0x}\Big[1+\varphi_{0y}\Big] \quad (y=f(x), |x|<1), \qquad \Re[\hat{w}_1] = 0 \quad (y=0, |x|>1). \tag{16}$$

In the problem of floating plate impact, where $\varphi_{0y} = -1$ on the plate, conditions (16) are homogeneous and $\hat{w}_1(z)$ is given as a superposition of eigenfunctions

$$\hat{w}_1(z,t) = \mathrm{i}\sum_{n=0}^{N_e} C_n(t)[\zeta^2-1]^{-\frac{2n+1}{2}}, \quad z = G(\zeta), \tag{17}$$

where $C_n(t)$ are real functions which should be determined together with the number of the eigenfunctions N_e taken into account by using the condition of matching the outer solution (5) with the inner solutions in a small vicinities of the intersection points, $x=\pm1$, $y=0$. In the following only the leading order terms of the outer and inner solutions are matched, this is why it will be enough to take $N_e = 0$ in (17).

By using Eqs. (7) and (9), we obtain

$$\varphi_{0x}[1+\varphi_{0y}] = \frac{G_\infty^2 f_x(x)}{[1+f_x^2(x)]^2}\,\frac{\xi^2}{(1-\xi^2)[x_\xi(\xi,0)]^2}, \quad x = x(\xi,0) \tag{18}$$

for an arbitrary symmetric body. The function $\varphi_{0x}[1+\varphi_{0y}](\xi,0)$, where $|\xi|<1$, is denoted below by $u(\xi)$. Note that $u(\xi) = \varphi_{0x}^2(\xi,0) f_x[x(\xi,0)]$. For a wedge the calculations provide

$$u(\xi) = \tfrac{1}{2}\sin(2\gamma)\,\mathrm{sgn}(\xi)|\xi|^{2-4\gamma/\pi}(1-\xi^2)^{2\gamma/\pi-1}, \tag{19}$$

where $-1<2\gamma/\pi-1<0$ and $0<2-4\gamma/\pi<2$. The function $u(\xi)$ is integrable.

For an arbitrary symmetric body the unknown function $\hat{w}_1(z,t)$ is equal to the sum of the particular solution

$$\hat{w}_{1P}(z) = \frac{\mathrm{i}}{\pi\sqrt{\zeta^2-1}}\int_{-1}^{1}\frac{\sqrt{1-\tau^2}u(\tau)\,\mathrm{d}\tau}{\tau-\zeta}, \quad z = G(\zeta) \tag{20}$$

and the eigensolution (17).

The pressure-impulse solution (5) and (8) provides a singular velocity field at the intersection points $x=\pm1$, $y=0$. Moreover, the complex potential $w_1(z,t)$ in (5) is singular itself. Therefore, the obtained solution has to be considered as the outer solution. The inner solution, which is used here to resolve this singularity, is derived in Section 5. In order to

formulate the matching conditions, the behaviour of the outer solution close to the intersection points has to be analyzed.

4. Outer solution near the intersection points

Near the right-hand side intersection point, $z = 1$, the conformal mapping behaves as

$$z - 1 = G_1(\zeta - 1)^{\beta/\pi} + G_2(\zeta - 1)^{2\beta/\pi} + \mathcal{O}[(\zeta - 1)^{\beta/\pi + 1}]. \tag{21}$$

The coefficient G_1 is dependent on the body shape,

$$G_1 = \lim_{\zeta \to 1} \frac{G(\zeta) - 1}{(\zeta - 1)^{\beta/\pi}},$$

$\beta = \pi - \gamma$ and the coefficient G_2 accounts for the effect of the body curvature close to the intersection point, $G_2 = f''(1)G_1^2 \cos^3\gamma/[2\sin\gamma]$. Inverting asymptotic formula (21), we find

$$\zeta - 1 = \left[\frac{z-1}{G_1}\right]^{2\sigma_0} \left\{1 - 2\sigma_0 \frac{G_2}{G_1^2}(z-1) + \mathcal{O}[|z-1|^{2\sigma_0}]\right\}, \quad \sigma_0 = \frac{\pi}{2\beta}. \tag{22}$$

In order to obtain the asymptotic formula for $\hat{w}_{1P}(z)$ as $z \to 1$, we decompose the product $\sqrt{1-\tau^2}u(\tau)$ in the integral (20) as

$$\sqrt{1-\tau^2}u(\tau) = S_1(1-\tau)^{\kappa} + U(\tau), \quad \kappa = \frac{2}{\pi}\left(\gamma - \frac{\pi}{4}\right), \quad S_1 = \frac{1}{\sqrt{2}}\left(\frac{\pi G_\infty}{\sqrt{2}\beta G_1}\right)^2 \sin(2\gamma),$$

where $U(\tau) = \mathcal{O}[(1-\tau)^{(\gamma/\pi)+(1/2)}]$ as $\tau \to 1 - 0$, and calculate

$$\int_{-1}^{1} \frac{\sqrt{1-\tau^2}u(\tau)\,\mathrm{d}\tau}{\tau - \zeta} = S_1 \int_{-1}^{1} \frac{(1-\tau)^{\kappa}\,\mathrm{d}\tau}{\tau - \zeta} + U_1 + \mathcal{O}[(1-\zeta)^{\frac{\gamma}{\pi}+\frac{1}{2}}], \quad U_1 = \int_{-1}^{1} \frac{U(\tau)\,\mathrm{d}\tau}{\tau - 1} \quad (\zeta \to 1). \tag{23}$$

Here

$$\begin{aligned}
\int_{-1}^{1} \frac{(1-\tau)^{\kappa}\,\mathrm{d}\tau}{\tau - \zeta} &= -\frac{2^{\kappa}}{\kappa} - \frac{\pi}{\cos(2\gamma)}\left[\frac{z-1}{G_1}\right]^{3\sigma_0 - 2} + \mathcal{O}[|z-1|^{3\sigma_0 - 1}] \quad \left(\gamma < \frac{\pi}{4}\right), \\
&= -\frac{2^{\kappa}}{\kappa} - \frac{\pi}{\cos(2\gamma)}\left[\frac{z-1}{G_1}\right]^{3\sigma_0 - 2} + \mathcal{O}[|z-1|^{2\sigma_0}] \quad \left(\gamma > \frac{\pi}{4}\right), \\
&= -\ln 2 + 2\sigma_0 \ln\left[\frac{z-1}{G_1}\right] + \mathcal{O}[|z-1|^{2\sigma_0}] \quad \left(\gamma = \frac{\pi}{4}\right).
\end{aligned}$$

By substituting (22) into Eq. (5) and using formulae (8), (15), (17), (20) and (23), we find for $\gamma \neq \frac{\pi}{4}$

$$\begin{aligned}
w(z,t) = \mathrm{i}\dot{h}(t)[1 - A(z-1)^{\sigma_0} + \mathcal{O}(|z-1|H) + h\dot{h}\Big[&-\frac{A^2\sigma_0^2}{2\cos(2\gamma)}\exp(2\mathrm{i}\gamma)(z-1)^{2\sigma_0 - 2} \\
&+ A\sigma_0(z-1)^{\sigma_0 - 1} + \mathrm{i}\mu_2(z-1)^{-\sigma_0} - \frac{1}{2} + o(1)\Big] + o(t),
\end{aligned} \tag{24}$$

where

$$A = \frac{\sqrt{2}G_\infty}{G_1^{\sigma_0}}, \quad \mu_2 = \frac{1}{\sqrt{2}}\left[C_0(t) + \frac{U_1}{\pi} - \frac{2^{\kappa}S_1}{\pi\kappa}\right]G_1^{\sigma_0}.$$

By taking the real part of asymptotic formula (24) in the local coordinates, $z = 1 + r\exp[\mathrm{i}(\theta - \beta)]$, where $r \ll 1$, $\theta = 0$ on the body surface and $\theta = \beta$ on the free surface, we obtain the asymptotic expansion of the outer velocity potential close to the intersection point in the form

$$\begin{aligned}
\varphi(x,y,t) = -\dot{h}(t)Ar^{\sigma_0}\cos(\sigma_0\theta) + \mathcal{O}(r) + h\dot{h}\Big[&\frac{1}{2}A^2\sigma_0^2 r^{2\sigma_0 - 2}\frac{\cos[(2\sigma_0 - 2)\theta]}{\cos(2\gamma)} \\
&+ A\sigma_0 r^{\sigma_0 - 1}\sin[(\sigma_0 - 1)\theta + \beta] - \mu_2 r^{-\sigma_0}\cos(\sigma_0\theta) - \frac{1}{2} + o(1)\Big] + o(t).
\end{aligned} \tag{25}$$

It should be noticed that the curvature of the body surface near the intersection points does not contribute to the derived asymptotics. The curvature contributes to the higher-order terms. The obtained asymptotic behaviour depends on the local deadrise angle. The only quantity in the asymptotics which is dependent on the global shape of the body, is the integral U_1 in (23).

It is seen that the outer solution predicts unbounded velocity of the flow close to the intersection points. The higher the order of the outer asymptotics, the higher is the singularity of the solution. The inner solution is required to improve the prediction of the flow pattern close to the intersection points and to derive an equation for the coefficient $C_0(t)$ of the eigensolution. The latter equation is of major importance to evaluate the initial asymptotics of the hydrodynamic force acting on the body. In the following section the first-order inner solution is obtained and matched to the first-order outer solution. An equation for the coefficient $C_0(t)$ is derived by matching the first-order inner solution with the second-order outer solution.

5. Inner solution about the intersection point

The vicinity of the right-hand side intersection point, $x = 1$, $y = 0$, is considered. The inner variables are introduced as (Fig. 3)

$$x = 1 + a(t)\lambda, \quad y = a(t)\mu, \quad r = a(t)\rho, \quad \eta(x,t) = a(t)H(\lambda,t), \quad \varphi = \dot{h}Aa^{\sigma_0}\varphi_i(\lambda,\mu,t), \quad p = \dot{h}^2 a^{2\sigma_0-2}A^2 p_i(\lambda,\mu,t). \tag{26}$$

The function $a(t)$, which defines the dimension of the inner region, is obtained from the condition of balance between linear and nonlinear terms in the inner solution

$$a(t) = [(2-\sigma_0)Ah(t)]^{\frac{1}{2-\sigma_0}}.$$

The inner pressure $p_i(\lambda,\mu,t)$ is given as

$$p_i = \lambda\varphi_{i\lambda} + \mu\varphi_{i\mu} - \sigma_0\varphi_i - \tfrac{1}{2}|\nabla\varphi_i|^2 + \mathcal{O}(h\ddot{h}). \tag{27}$$

By using Eqs. (1) and (2), the boundary-value problem for the inner velocity potential is obtained in the form

$$\begin{aligned}
&\Delta\varphi_i = 0 \quad (\text{in } \Omega_i),\\
&\lambda\varphi_{i\lambda} + \mu\varphi_{i\mu} - \sigma_0 + \tfrac{1}{2}|\nabla\varphi_i|^2 = \mathcal{O}(h\ddot{h}) \quad (\mu = H(\lambda,t)),\\
&\varphi_{i\mu} = H_\lambda\varphi_{i\lambda} + H - \lambda H_\lambda + \mathcal{O}(h) \quad (\mu = H(\lambda,t)),\\
&\frac{\partial\varphi_i}{\partial n} = \mathcal{O}(h^{\frac{1-\sigma_0}{2-\sigma_0}}) \quad (\mu = \lambda\tan\gamma),\\
&\varphi_i \sim -\rho^{\sigma_0}\cos(\sigma_0\theta) \quad (\rho\to\infty).
\end{aligned} \tag{28}$$

Eqs. (28) imply that in the leading order as $t \to 0$ the inner flow is nonlinear and self-similar.

The boundary-value problem (28) is identical to that studied by Iafrati and Korobkin (2004) for the floating wedge case. In particular, in that analysis the asymptotic behaviour of the inner velocity potential in the far field, $\rho \to \infty$, was recovered as

$$\varphi_i(\rho,\theta) = -\rho^{\sigma_0}\cos(\sigma_0\theta) + C_E\rho^{-\sigma_0}\cos(\sigma_0\theta) + \frac{\sigma_0^2}{2-\sigma_0}\frac{\cos[2(1-\sigma_0)\theta]}{2\cos(2\gamma)}\rho^{2(\sigma_0-1)} + o(\rho^{2(\sigma_0-1)}) + \mathcal{O}(h^{\frac{1-\sigma_0}{2-\sigma_0}}), \tag{29}$$

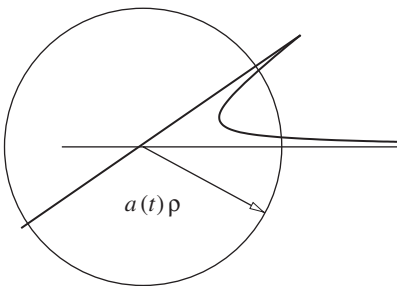

Fig. 3. Definition of the inner region.

where $\gamma \neq \frac{\pi}{4}$. The case $\gamma = \pi/4$ was studied in Iafrati and Korobkin (2002). The second term in (29) with the coefficient C_E represents the eigensolution of the inner problem (28) in the far field. This term is of higher order than the third term in (29) for $\gamma > \pi/4$. Therefore, for a deadrise angle greater than 45° the second term has to be removed from the asymptotic formula (29). If $0 < \gamma < \frac{\pi}{4}$ this term gives an important contribution to the far-field asymptotics and the coefficient C_E should be evaluated numerically together with the solution of the boundary-value problem (28). Note that in the case $\pi/4 < \gamma < \pi/2$ the coefficient C_E of the second term in (29) can also be evaluated numerically; however, due to the high order of this term, the calculations were found to be unreliable.

The asymptotics (25) and (29) have to match each other up to the designated higher order terms. By substituting $r = a(t)\rho$ into Eq. (25) and dividing the result by scale factor $\dot{h}Aa^{\sigma_0}$, we obtain

$$\frac{\varphi(1 + a(t)\lambda, a(t)\mu, t)}{\dot{h}Aa^{\sigma_0}} = -\rho^{\sigma_0}\cos(\sigma_0\theta) + \frac{\sigma_0^2}{2-\sigma_0}\frac{\cos[2(1-\sigma_0)\theta]}{2\cos(2\gamma)}\rho^{2(\sigma_0-1)} - \tilde{\mu}_2 h^{\chi}\rho^{-\sigma_0}\cos(\sigma_0\theta) + \mathcal{O}(h^{\frac{2-2\sigma_0}{2-\sigma_0}}), \tag{30}$$

where

$$\tilde{\mu}_2 = \mu_2 A^{-\frac{2+\sigma_0}{2-\sigma_0}}(2-\sigma_0)^{-\frac{2\sigma_0}{2-\sigma_0}}, \quad \chi = \frac{2-3\sigma_0}{2-\sigma_0}.$$

Note that $\chi < \frac{2-2\sigma_0}{2-\sigma_0}$ for any value of σ_0, $\frac{1}{2} < \sigma_0 < 1$.

The right-hand sides in (29) and (30) should be equal and therefore the matching condition provides

$$\tilde{\mu}_2 = -C_E h^{-\chi} \quad \left(0 < \gamma < \frac{\pi}{4}\right), \tag{31}$$

from which the formula for the coefficient C_0 in (17) is derived as

$$C_0 = -\tilde{C}_E h^{\frac{3\sigma_0-2}{2-\sigma_0}} + \frac{2^{\kappa}S_1}{\pi\kappa} - \frac{U_1}{\pi}, \quad \tilde{C}_E = \sqrt{2}C_E G_1^{-\sigma_0}A^{\frac{2+\sigma_0}{2-\sigma_0}}(2-\sigma_0)^{\frac{2\sigma_0}{2-\sigma_0}} \left(0 < \gamma < \frac{\pi}{4}\right). \tag{32}$$

For larger deadrise angles, $\pi/4 < \gamma < \pi/2$, Eq. (32), formally speaking, can also be used. However, the coefficient C_E in (29) for $\pi/4 < \gamma < \pi/2$ is rather difficult to evaluate numerically as the eigensolution in this case is of higher order.

6. Asymptotics of the hydrodynamic force on the moving body

Eqs. (3), (5), (13) and (15) provide as $t \to 0$ that outside of small vicinities of the intersection points the pressure along the surface of the moving body is given by

$$p(x, f(x) - h(t), t) = -\ddot{h}\varphi_0(x, f(x)) - \dot{h}^2[\varphi_{0x}^2(x, f(x)) + \hat{\varphi}_1(x, f(x), t)] - h\dot{h}\hat{\varphi}_{1t}(x, f(x), t) - \mathrm{Fr}^{-2}y + o(1), \tag{33}$$

where $\hat{\varphi}_1(x, f(x), t)$ is presented in the parametric form as

$$\hat{\varphi}_1(x, f(x), t) = -\frac{C_0(t)}{\sqrt{1-\xi^2}} - \frac{1}{\pi\sqrt{1-\xi^2}}\int_{-1}^{1}\frac{\sqrt{1-\tau^2}u(\tau)\,\mathrm{d}\tau}{\tau - \xi}, \quad x = x(\xi, 0) \ (|\xi| < 1).$$

Note that even if the inner pressure is very high compared with the pressure in the outer region, the contribution of the inner pressure to the hydrodynamic force after the impact tends to zero as $t \to 0$. This contribution is of the order $\mathcal{O}(pa)$, where the order of the hydrodynamic pressure in the inner region is defined in (26), thus $\mathcal{O}(pa) = \mathcal{O}(\dot{h}^2 a^{2\sigma_0-1}A^2) = \mathcal{O}(\dot{h}^2 h^{(2\sigma_0-1)/(2-\sigma_0)}) = o(1)$. We may conclude that the contribution $F_{in}(t)$ of the inner pressure to the hydrodynamic force in the leading order is

$$F_{in}(t) = C_1\dot{h}^2 h^{\frac{2\sigma_0-1}{2-\sigma_0}}(1 + o(1)), \tag{34}$$

where the constant factor C_1 should be calculated by integrating the inner pressure in small vicinities of the intersection points. Therefore, up to the terms which tend to zero as $t \to 0$, the initial asymptotics of the hydrodynamic force are determined by the pressure distribution in the outer region. From the asymptotic behaviour of φ_0 and $\hat{\varphi}_1$ the outer pressure about the intersection point follows as

$$p \sim \dot{h}^2\left[\mu_2 r^{-\sigma_0} - A^2\sigma_0^2\frac{\cos^2\gamma}{\cos(2\gamma)}r^{2\sigma_0-2}\right] + \dot{h}h\dot{\mu}_2 r^{-\sigma_0} + o(1) \quad (r \to 0),$$

where r is the distance from the intersection point along the body contour. By using Eqs. (32), we finally get

$$p \sim \dot{h}^2 \left[\frac{2\sigma_0}{2-\sigma_0}\, \mu_2 r^{-\sigma_0} - A^2 \sigma_0^2\, \frac{\cos^2\gamma}{\cos(2\gamma)} r^{2\sigma_0-2} \right] + o(1) \quad (r \to 0),$$

which shows that the outer pressure field is singular about the intersection point, although the singularity is integrable. It is worth noticing that, in the latter asymptotic formula, both the distance r and the time t are small. Close to the intersection point it is reasonable to consider this pressure asymptotic expression within the inner variables, where $r = a(t)\rho$, $a(t) \ll 1$, $\rho \gg 1$ and $\rho a(t) \ll 1$. By using (31), we obtain the behaviour of the outer pressure as

$$p \sim \dot{h}^2 a^{2\sigma_0-2} A^2 \left[-2\sigma_0 C_E \rho^{-\sigma_0} - \sigma_0^2\, \frac{\cos^2\gamma}{\cos(2\gamma)} \rho^{2\sigma_0-2} \right] \quad (\rho \gg 1).$$

For $\pi/4 < \gamma < \pi/2$, we find $2\sigma_0 - 2 > -\sigma_0$, so that the second term in the asymptotic formula provides the main contribution to the pressure, where $\cos(2\gamma) < 0$. This implies that the pressure grows when approaching the intersection point from the outer region. The same is true for $0 < \gamma < \pi/4$. Indeed, in this case $2\sigma_0 - 2 < -\sigma_0$ and the first term provides the main contribution. This contribution is positive because $C_E < 0$, as was shown by Iafrati and Korobkin (2004).

By substituting (33) and (34) into Eq. (4), we obtain the dynamic component of the force as

$$F(t) = \ddot{h} M_a - \dot{h}^2 G_\infty [G_\infty E - \pi C_0(t)] + h\dot{h}\pi G_\infty \dot{C}_0(t) + C_1 \dot{h}^2 h^{\frac{2\sigma_0-1}{2-\sigma_0}} + o(1) \tag{35}$$

with

$$E = \int_{-1}^{1} \frac{\tau^2\, \mathrm{d}\tau}{(1-\tau^2) x_\xi(\tau, 0)[1 + f_x^2]}, \quad M_a = \pi G_\infty (G_0 + G_\infty/2) - S_w,$$

where M_a is the added mass of the body, S_w is the area of the submerged part of the body and, from Eqs. (32),

$$\dot{C}_0(t) = -\left(\frac{3\sigma_0 - 2}{2-\sigma_0} \right) \tilde{C}_E \dot{h} h^{\frac{4(\sigma_0-1)}{2-\sigma_0}}.$$

Eq. (35) indicates than the two terms in Eq. (35) containing $C_0(t)$ and $\dot{C}_0(t)$ are of the same order in h, which is $\mathcal{O}(h^{(3\sigma_0-2)/(2-\sigma_0)})$.

The first term in (35) represents the well-known result of pressure-impulse theory. The hydrodynamic force acting on a body, which starts to move, is equal to the product of the body added mass M_a and the body acceleration $\ddot{h}$ during the impact. If the body moves after its impulsive start with a constant velocity, $\dot{h} = 1$, when $t > 0$, the first term in (35) is equal to $M_a \delta(t)$, where $\delta(t)$ is the Dirac delta-function, and gives no contribution to the force for $t > 0$. Hence, in this case the asymptotics of the hydrodynamic force take the form

$$F(t) = -G_\infty \left[G_\infty E - \pi \left(\frac{2^k S_1}{\pi k} - \frac{U_1}{\pi} \right) \right] - \pi G_\infty \tilde{C}_E\, \frac{2\sigma_0}{2-\sigma_0}\, t^{\frac{3\sigma_0-2}{2-\sigma_0}} + C_1 t^{\frac{2\sigma_0-1}{2-\sigma_0}} + o(1). \tag{36}$$

Eq. (36) highlights the important role played by the eigensolution of the inner problem, the coefficient of which explicitly appears in the first time-dependent term. Note that the correction term with C_1 related to the inner pressure field has been introduced in (35) and (36) even though this term is of higher order than other displayed terms.

With the aim of establishing a comparison between the theoretical findings and numerical results, Eq. (36) is specialized for a floating wedge, which starts suddenly to move down at a constant velocity, $\dot{h} = 1$. For a wedge, we have

$$E = \frac{\pi - 2\gamma}{\tan\gamma}, \quad G_\infty = \frac{1}{w\cos\gamma}, \quad w = \frac{1}{\sqrt{\pi}}\, \Gamma\left(\frac{1}{2} + \frac{\gamma}{\pi} \right) \Gamma\left(1 - \frac{\gamma}{\pi} \right)$$

and

$$\left(\frac{2^k S_1}{\pi k} - \frac{U_1}{\pi} \right) = \frac{\sin(2\gamma)}{2\pi}\, \frac{\Gamma\left(\frac{3}{2} - \kappa\right) \Gamma(\kappa)}{\Gamma\left(\frac{3}{2}\right)}.$$

We do not evaluate the coefficient C_1 in the present analysis. The constant $\tilde{C}_E$ is given in Eq. (32) where, for the wedge case,

$$G_1 = 2^{\left(1-\frac{\gamma}{\pi}\right)} \sigma_0 G_\infty.$$

In the asymptotic expression (36) of the hydrodynamic force three terms can be recognized. In addition to the time independent part

$$F_0 = -G_\infty \left[G_\infty E - \pi \left(\frac{2^k S_1}{\pi k} - \frac{U_1}{\pi} \right) \right], \tag{37}$$

two time-dependent terms $F_1(t)$ and $F_2(t)$, which originate from the inner solution and its matching with the outer solution, appear

$$F_1(t) = C_1 t^{\frac{2\sigma_0 - 1}{2-\sigma_0}}, \quad F_2(t) = -\pi G_\infty \frac{2\sigma_0}{2-\sigma_0} \tilde{C}_E t^{\frac{3\sigma_0 - 2}{2-\sigma_0}}. \tag{38}$$

While $F_1(t)$ always tends to zero as $t \to 0$, the term $F_2(t)$ has the power $(3\sigma_0 - 2)/(2 - \sigma_0)$, which is negative as $\gamma < \pi/4$. As a result, while the hydrodynamic force starts at $t = 0$ from the finite value F_0 for $\gamma > \pi/4$, for smaller deadrise angles the term $F_2(t)$ is responsible for unbounded loads as $t \to 0$. With the aim of clarifying the last statement, it is worth noticing that the unbounded loads as $t \to 0$ are caused by the eigensolution term appearing in the inner velocity potential. The power of the eigensolution term is negative for $\gamma < \pi/4$. This means that the hydrodynamic force is unbounded as time tends to zero because the pressure given by Eq. (33) diverges due to the behaviour of both $\hat{\phi}_1$ and $h\hat{\phi}_{1t}$ as $t \to 0$. In the case $\gamma = \pi/4$, the form of the inner solution is significantly different from that found for $\gamma \neq \pi/4$ and also the matching procedure differs. Analysis of this case is more sophisticated than that presented in this paper [for details of the analysis see Iafrati and Korobkin, 2002].

7. Numerical modelling

The analysis presented above provides important insights on the hydrodynamic loads acting on the surface of the entering body. However, the hydrodynamic loads can also be evaluated with the help of unsteady fully nonlinear numerical approaches. Nowadays such kinds of tool are becoming more and more accurate and reliable and their flexibility is making them widely adopted. Nevertheless, some problems still exist which cannot be treated satisfactorily with the commonly adopted approaches. The early stage after the sudden start of a floating body is one of them.

In order to explain reasons that make this problem difficult to handle by using classical numerical approaches, a brief discussion of their basic principles is worthwhile. Most of the fully nonlinear numerical approaches are based on the mixed Eulerian–Lagrangian formulation, originally proposed by LonguetHiggings and Cokelet (1976). At each time step the flow velocity potential is found by solving a boundary problem with a Dirichlet condition imposed on the free surface and a Neumann condition assigned along the solid boundaries. From the solution of this boundary value problem, usually achieved through panel methods, the velocity potential along the body contour and its normal derivative along the free surface are derived, thus making it possible to evaluate the velocity components on the free surface. Then the free surface is advanced in time by integrating the velocity field to get the new free surface position and the unsteady Bernoulli equation is used to get the velocity potential along it.

The difficulties that this approach encounters when simulating the water entry of an initially floating flared body can be easily understood by looking at the sketch shown in Fig. 4, where the discretization about the initial configuration is shown near the intersection point. The boundary condition enforced on the solid boundary, $\partial\varphi/\partial n = \cos\gamma$, and on the free surface, $\varphi = 0$, do not match each other at the intersection point, giving rise to the flow singularity discussed in Section 2, and leading to the development of a thin jet. During the early stage after the body start, numerical simulations are not able to describe this singularity and the predicted hydrodynamic loads are not reliable. Later on, the jet develops, removing the flow singularity and thus making the hydrodynamic loads reliable (Iafrati et al., 2000; Battistin and Iafrati, 2003).

Owing to the limitations of boundary element approaches when describing the flow inside thin jets, rather simplified models are often adopted which cut the thin jet off the computational domain (Zhao and Faltinsen, 1993). Although

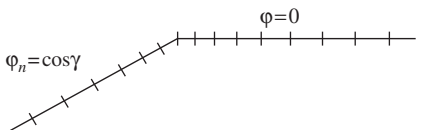

Fig. 4. Sketch of the discretization adopted about the intersection point. The mismatch of the boundary conditions is responsible for the jet development.

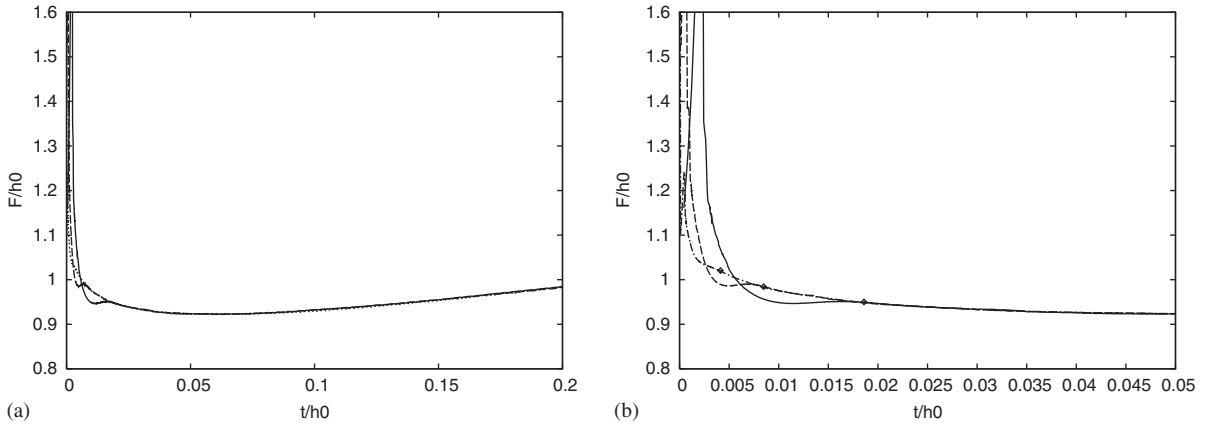

Fig. 5. History of the hydrodynamic loads for a floating wedge with $\gamma = 60^\circ$. On (b) diamonds denote the lower limit of reliability of the time histories. Key: $A_0/h_0 = 0.018042725$ (solid), 0.009021363 (dash), 0.004510681 (dash-dot).

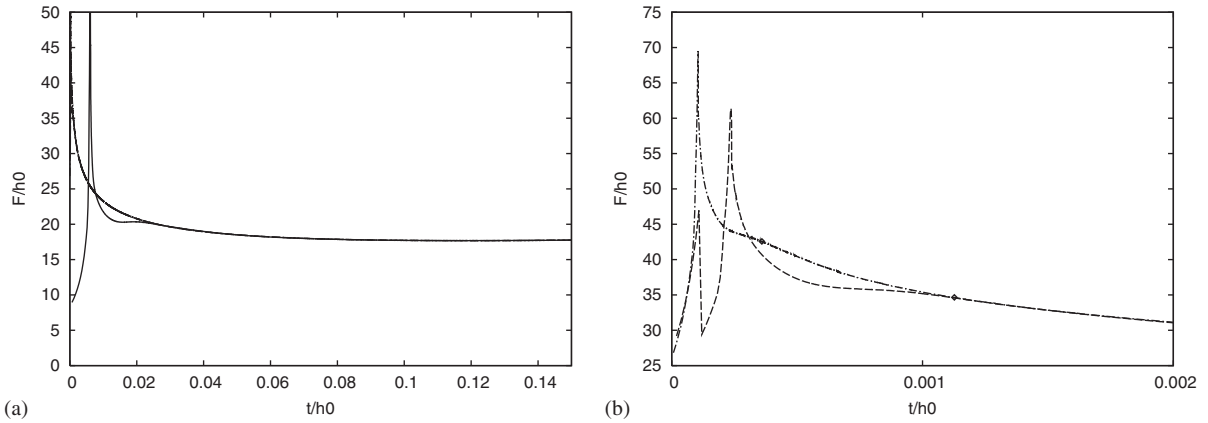

Fig. 6. History of the hydrodynamic loads for a floating wedge with $\gamma = 30^\circ$. On (b) diamonds denote the lower limit of reliability of the time histories. Key: $A_0/h_0 = 0.09237875$ (solid), 0.009237875 (dash), 0.004618937 (dash-dot).

more accurate models were developed (Battistin and Iafrati, 2004), even the very simple models are rather appropriate when attention is mainly devoted to the hydrodynamic loads, since the pressure inside the thin jet layer is about zero. This is why in the following the numerical model described in Battistin and Iafrati (2003) is adopted to compute the unsteady flow generated by the water entry of a wedge initially floating on the free surface. Simulations are performed for two different deadrise angles, $\gamma = 30^\circ$ and $\gamma = 60^\circ$. For both cases several simulations are performed for different grid refinements. The discretization of the free surface is started at the intersection point and the panel size is progressively increased while moving toward the far field. In the following, each numerical simulation is characterized in terms of the initial length A_0 of the first free surface panel attached to the body. Reduction of this parameter makes the vertical velocity at the first panel larger and the early stage, during which the solution is not reliable, shorter. The numerical simulations, which are carried out for constant entry velocity $V_0 = 1$, last until the vertical displacement of the wedge apex is twice the initial apex submergence.

The hydrodynamic loads provided by the numerical simulations for $\gamma = 60^\circ$, are shown, in nondimensional form, in Fig. 5. For this case three numerical simulations are carried out by using three different panel sizes obtained by halving twice the value used for the coarsest case, which is $A_0/h_0 = 0.018042725$. Fig. 5(a) shows that the three curves overlap very well, aside from the very early part. For the latter, a close-up view is depicted in Fig. 5(b), where marks denote the points starting from which the time histories can be considered reliable. The same comparison is established in Fig. 6 for the wedge with $\gamma = 30^\circ$. For this set of calculations the coarsest grid A_0/h_0 is 20 times larger than that used for the

Table 1
Coefficients of the expansion (39) found through least-squares approximations of the numerical data

	Value ($\gamma = 30^\circ$)	Error % ($\gamma = 30^\circ$)	Value ($\gamma = 60^\circ$)	Error % ($\gamma = 60^\circ$)
a	−15.4897	0.0672	2.35994	0.0779
b	10.8574	0.0207	−2.03773	0.3513
c	12.8762	0.0906	1.13076	0.6304
d	14.4686	0.0633	0.72610	0.2722

Least-squares interpolation has been established in the range $t/h_0 = (0.0004, 0.5)$ for the case $\gamma = 30^\circ$ and $t/h_0 = (0.005, 0.5)$ for the case $\gamma = 60^\circ$.

Table 2
Results provided by least-squares interpolation on a larger time interval $t/h_0 = (0.0004, 2)$ for the case $\gamma = 30^\circ$ and $t/h_0 = (0.005, 2)$ for the case $\gamma = 60$

	Value ($\gamma = 30^\circ$)	Error % ($\gamma = 30^\circ$)	Value ($\gamma = 60^\circ$)	Error % ($\gamma = 60^\circ$)
a	−16.5367	0.0403	2.32808	0.0709
b	11.0743	0.0147	−1.92133	0.2764
c	14.0958	0.0453	1.02564	0.4157
d	13.4999	0.0121	0.744796	0.0770

finest one. The singularity is much more pronounced in this case, which makes the duration of the initial stage much shorter with respect to that for $\gamma = 60^\circ$.

The reliable parts of the force histories can be used to derive, with the help of the least-squares approximation, the coefficients in expansion (36) once the expansion is presented in the form

$$F(t) \sim a + bt^{\frac{3\sigma_0-2}{2-\sigma_0}} + ct^{\frac{2\sigma_0-1}{2-\sigma_0}} + dt. \tag{39}$$

The last term in (39) has been introduced to account for the linear behaviour that characterizes the self-similar solution of the wedge entry problem. In fact, in both cases shown above, the linear trend is progressively approached when the body displacement $V_0 t$ exceeds one third of the initial submergence h_0 .

The coefficients of Eq. (39) evaluated through the least-squares interpolation of the numerical results are reported in Tables 1 and 2 along with the corresponding errors in percent. The least-squares fit established on different portions of the time history gives differences in the estimated coefficients which are rather large for the case $\gamma = 30^\circ$ (up to 10%) while they are much less for the case $\gamma = 60^\circ$. This is caused by the unbounded values that the second term in (39) takes as $t \to 0$ for $\gamma = 30^\circ$. For $\gamma = 30^\circ$, the coefficient d of the linear term provided by the least-squares fit is not far from the value predicted by Zhao and Faltinsen (1993) on the basis of the similarity solution, which is 14.139 (Tables 1 and 2).

Evaluation of the time independent term in (39) directly from Eq. (37) provides

$$a(\gamma = 30^\circ) = -10.5038, \quad a(\gamma = 60^\circ) = 2.38057.$$

These formulae show that, while the value of a in (39) for $\gamma = 60^\circ$ is rather close to the estimate provided by the least-squares fit, that for $\gamma = 30^\circ$ is significantly different. This can be attributed to the divergent behaviour of the second term in expansion (39), which is of higher order than the first one for $\gamma > 45^\circ$. It is possible to obtain a better agreement between the analytical and numerical results for $\gamma = 30^\circ$ by performing numerical calculations with finer discretization. If so, the region along which the least-squares fitting is established will be extended towards $t = 0$. However, the discretization adopted in the present numerical calculation is already very refined and a further refinement would be very expensive.

By using the coefficient b provided by the least-squares fit for $\gamma = 30^\circ$, through Eqs. (38) and (32), the constant C_E of the eigensolution can be evaluated as $C_E = -0.888$. This value differs from the value $C_E = -0.6795$ derived from the solution of the inner problem in Iafrati and Korobkin (2004). The understanding of reasons for this disagreement needs a deeper investigation.

8. Discussion

The analysis presented above can be summarized as follows: (i) the leading order terms governing the initial asymptotics of the hydrodynamic loads acting on a floating flared body, which suddenly starts to move, have been recovered; (ii) the inner solution has been found to be responsible for the first two time-dependent terms appearing in the small time expansion of the hydrodynamic loads; (iii) in contrast to classical small time expansions, these time-dependent terms have non-integer powers of time; (iv) for deadrise angles smaller than 45°, negative powers of time appear which are responsible for the unbounded behaviour of the hydrodynamic loads as $t \to 0$; (v) for deadrise angle at the water line larger than 45° the constant term representing the hydrodynamic load at $t \to 0$ has been derived.

These results can be used in numerical calculations of the free motion of floating bodies to overcome difficulties with accurate evaluation of the hydrodynamic loads during the early stage of the simulations. These loads, as discussed in Vinje (1994), may play an important role in prediction of the body motion for large time.

The idea is to perform a preliminary numerical simulation for the floating body by assuming a constant entry velocity. The dynamics of the body motion are not computed at this step. The numerical simulation has to be performed for an interval of time large enough to get a reasonably good estimate of the coefficients in Eq. (39) through least-squares fit of the predicted hydrodynamic loads. Numerical simulations with finer resolutions can be done with the aim of evaluating the reliable extent of the time history, which has to be used for the fitting.

Once the coefficients a, b, c and d in (39) have been evaluated, we present the hydrodynamic force acting on the free moving body just after the impact as

$$F(t) = \ddot{h} M_a + a\dot{h}^2 + b\dot{h}^2 h^{\frac{3\sigma_0-2}{2-\sigma_0}} + c\dot{h}^2 h^{\frac{2\sigma_0-1}{2-\sigma_0}} + d\dot{h}^2 h, \tag{40}$$

where the added mass M_a is evaluated analytically or numerically for the initial shape of the submerged part of the body. Eq. (40) follows from comparison of Eqs. (39) and (35). Note that the coefficients in (40) were calculated from the solution of the auxiliary problem of the body motion at constant speed, $\dot{h} = 1$, in non-dimensional variables.

Free body motion after impact is governed in the non-dimensional variables by the equation

$$M_b \ddot{h} = -F(t), \tag{41}$$

where the hydrodynamic force $F(t)$ is given by (40), $M_b = m/\varrho_0 L^2$, m is the body mass per unit length, ϱ_0 is the water density and L is the half-width of the body at the water level. The differential equation (41) is solved together with the initial conditions

$$h(0) = 0, \quad \dot{h}(0) = 1. \tag{42}$$

Eq. (41) can be integrated once by using the substitution

$$\dot{h} = \exp[U(h)], \quad U(0) = 0. \tag{43}$$

We find

$$U(h) = -\frac{1}{M_b + M_a}\left(ah + b\,\frac{2-\sigma_0}{2\sigma_0}\,h^{\frac{2\sigma_0}{2-\sigma_0}} + c\,\frac{2-\sigma_0}{1+\sigma_0}\,h^{\frac{1+\sigma_0}{2-\sigma_0}} + \frac{1}{2}\,dh^2\right). \tag{44}$$

Finally, we calculate the function $t = t(h)$ as

$$t = \int_0^h \exp[-U(\xi)]\,\mathrm{d}\xi. \tag{45}$$

During the early stage of the body displacement $h(t)$ after the impact, its velocity $\dot{h}(t)$ and acceleration $\ddot{h}(t)$, as well as the hydrodynamic force $F(t)$, are obtained by using Eqs. (40), (41) and (43)–(45). Calculations based on this analytic solution are used for small penetration depths until the numerical simulation of the auxiliary problem becomes reliable. Starting from this depth, the analytic solution is replaced by the numerical solution provided by an unsteady solver. As an example, such calculations are performed for both $\gamma = 30°$ and $\gamma = 60°$ for two different masses of the impacting body, $M_b = 10$ and $M_b = 100$. Calculations last until the body displacement is one half of the initial apex submergence. Results, shown in Fig. 7, are compared with the corresponding time histories for the constant entry velocity case, which is the limit as $M_b \to \infty$. The important role played by the mass of the impacting body is clearly highlighted.

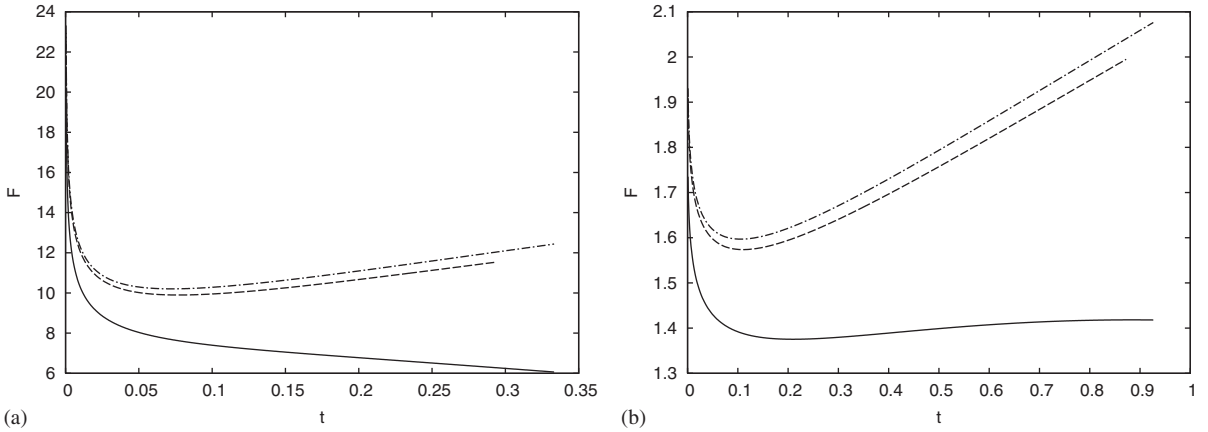

Fig. 7. Time histories of the total impacting load obtained from the integration of the dynamic of the body motion given by Eq. (41) for $\gamma = 60^\circ$ (a) and $\gamma = 30^\circ$ (b). Calculations are carried out for $M_b = 10$ (solid), $M_b = 100$ (dash) and results are compared with the time history in the constant entry velocity case, which corresponds to the limit value as $M_b \to \infty$ (dash-dot).

Before closing this section, it is worth remarking that similar calculations could be done in order to investigate the role played by the gravity term, thus providing an *a posteriori* verification of the initial assumption.

9. Conclusions

The small time asymptotics of the hydrodynamic loads generated after the sudden vertical motion of initially floating bodies has been investigated. In this respect, it has been shown that a very important role is played by the details of the body shape at the intersection with the water line. It has been found that the details of the flow about the intersection points govern the leading terms in the small time expansion of the loads. In particular, in contrast to the common understanding of expansions, it has been shown that the inner solution is directly responsible for non-integer powers of time, which only depend on the deadrise angle at the water line. Furthermore, for deadrise angle smaller than 45°, the leading term has a negative power in time and is responsible for unbounded loads as $t \to 0$. For deadrise angles larger than 45°, the hydrodynamic load as $t \to 0$ is found to be bounded and the asymptotic value for $t \to 0$ has been analytically derived. The theoretical value has been found to be in rather good agreement with that predicted by interpolation of the fully nonlinear numerical simulations.

Some physical intuitive arguments can be helpful in explaining a reason for the different nature of the initial solution depending on the deadrise angle of the body at the waterline. When the body deadrise angle is large enough, the liquid free surface is more able to be deformed, owing to the floating body impact. Hence, it is easier for the liquid to escape from the impact region and to develop the jets which contribute to evacuating the energy from the liquid surrounding the impulsively moving body. This implies a reduction of the hydrodynamic loads shortly after the impact. On the contrary, for relatively small deadrise angles, the part of the floating body which is initially above the water surface, restricts more strongly the free surface motion and the outflow of the liquid from the impact region surrounding the wetted part of the body. Roughly speaking, for small deadrise angles the water is trapped in the impact region and is much less free to flow toward the free surface. It is worth remarking that the non-integer powers in the initial asymptotics of the loads come from the inner region. This means that a special shape of the floating body at the waterline may help the liquid to escape from the impact region, thus allowing a reduction of the hydrodynamic loads. A practical conclusion from this observation can be formulated as follows: the deadrise angle of a floating body along its waterline must be (locally) as large as possible, in order to reduce the hydrodynamic loads caused by impulsive motion of the body.

Acknowledgements

Part of this work has been done during the stay of A. Iafrati at the Lavrentyev Institute of Hydrodynamics. The financial support provided by the Italian CNR NATO Fellowship (Bando N. 217.35 del 30/04/2003) is gratefully

acknowledged. The authors wish to thank the referees for their valuable comments and important suggestions, which improved the presentation.

References

Battistin, D., Iafrati, A., 2003. Hydrodynamic loads during water entry of two-dimensional and axisymmetric bodies. Journal of Fluids and Structures 17, 643–664.

Battistin, D., Iafrati, A., 2004. A numerical model for the jet flow generated by water impact. Journal of Engineering Mathematics 48, 353–374.

Faltinsen, O.M., 1977. Numerical solutions of transient nonlinear free-surface motion outside and inside moving bodies. In: Wehausen, J.V., Salvesen, N. (Eds.), Proceedings of the Second International Conference on Numerical Ship Hydrodynamics, Berkeley CA, USA, pp. 347–357.

Iafrati, A., Korobkin, A.A., 2002. Hydrodynamic loads at the early stage of a floating wedge impact. Proceedings of the Seventeenth International Workshop on Water Waves and Floating Bodies (IWWWFB), Cambridge, UK.

Iafrati, A., Korobkin, A.A., 2004. Starting flow generated by the impulsive start of a floating wedge. Journal of Engineering Mathematics 52, 99–126.

Iafrati, A., Carcaterra, A., Ciappi, E., Campana, E.F., 2000. Hydroelastic analysis of a simple oscillator impacting the free surface. Journal of Ship Research 44, 278–289.

King, A.C., Needham, D.J., 1994. The initial development of a jet caused by fluid, body and free-surface interaction. Part 1. A uniformly accelerating plate. Journal of Fluid Mechanics 268, 89–101.

Korobkin, A.A., Pukhnachov, V.V., 1988. Initial stage of water impact. Annual Review of Fluid Mechanics 10, 159–185.

Korobkin, A.A., Wu, G.X., 2002. Impact on a floating circular cylinder. Proceedings of the Royal Society, London A 456, 2489–2514.

Longuet-Higgings, M.S., Cokelet, E.D., 1976. The deformation of steep surface waves on water. I. A numerical method. Proceedings of the Royal Society, London A 350, 1–26.

Moyo, S., 1996. Hydrodynamic interaction of horizontal circular cylinders with a free-surface. Ph.D. Thesis, Brunel University, Department of Mathematics and Statistics.

Oliver, J.M., 2002. Water entry and related problems. Ph.D. Thesis, University of Oxford.

Tyvand, P., Miloh, T., 1995. Free surface flow due to impulsive motion of a submerged circular cylinder. Journal of Fluid Mechanics 286, 67–101.

Vinje, T., 1994. On small-time expansion of nonlinear free surface problems. Journal of Engineering Mathematics 28, 173–190.

Vinje, T., Brevig, P., 1980. Non-linear, two-dimensional ship motion. SIS Report, Norwegian Hydrodynamic Laboratory, Trondheim, Norway.

Zhao, R., Faltinsen, O.M., 1993. Water entry of two-dimensional bodies. Journal of Fluid Mechanics 246, 593–612.